

Mapping of the air–sea CO₂ flux in the Arctic Ocean and its adjacent seas: Basin-wide distribution and seasonal to interannual variability



Sayaka Yasunaka^{a, b, *}, Akihiko Murata^{a, b}, Eiji Watanabe^b, Melissa Chierici^{c, d},
Agneta Fransson^e, Steven van Heuven^f, Mario Hoppema^g, Masao Ishii^h,
Truls Johannessenⁱ, Naohiro Kosugi^h, Siv K. Lauvset^j, Jeremy T. Mathis^k,
Shigeto Nishino^b, Abdurahman M. Omar^l, Are Olsenⁱ, Daisuke Sasano^h, Taro Takahashi^m,
Rik Wanninkhofⁿ

^a Research and Development Center for Global Change, Japan Agency for Marine–Earth Science and Technology, Japan

^b Institute of Arctic Climate and Environment Research, Japan Agency for Marine–Earth Science and Technology, Japan

^c Institute of Marine Research, Tromsø, Norway

^d Department of Marine Sciences, University of Gothenburg, Göteborg, Sweden

^e Norwegian Polar Institute, Fram Centre, Tromsø, Norway

^f Royal Netherlands Institute for Sea Research, Marine Geology and Chemical Oceanography, Netherlands

^g Alfred Wegener Institute Helmholtz Centre for Polar and Marine Research, Climate Sciences Department, Bremerhaven, Germany

^h Geochemistry and Oceanography Research Department, Meteorological Research Institute, Japan Meteorological Agency, Japan

ⁱ Geophysical Institute, University of Bergen and Bjerknes Centre for Climate Research, Bergen, Norway

^j Uni Research Climate, Bjerknes Centre for Climate Research, Bergen, Norway

^k NOAA Arctic Research Program, USA

^l Uni Research AS, Bergen, Norway

^m Lamont–Doherty Earth Observatory of Columbia University, Palisades, NY, USA

ⁿ Atlantic Oceanographic and Meteorological Laboratory, National Oceanographic and Atmospheric Administration, USA

ARTICLE INFO

Article history:

Received 30 November 2015

Received in revised form

23 February 2016

Accepted 31 March 2016

Available online 1 April 2016

Keywords:

Arctic Ocean

CO₂ flux

Self-organizing map

ABSTRACT

We produced 204 monthly maps of the air–sea CO₂ flux in the Arctic north of 60°N, including the Arctic Ocean and its adjacent seas, from January 1997 to December 2013 by using a self-organizing map technique. The partial pressure of CO₂ (pCO₂) in surface water data were obtained by shipboard underway measurements or calculated from alkalinity and total inorganic carbon of surface water samples. Subsequently, we investigated the basin-wide distribution and seasonal to interannual variability of the CO₂ fluxes. The 17-year annual mean CO₂ flux shows that all areas of the Arctic Ocean and its adjacent seas were net CO₂ sinks. The estimated annual CO₂ uptake by the Arctic Ocean was 180 TgC yr^{−1}. The CO₂ influx was strongest in winter in the Greenland/Norwegian Seas (>15 mmol m^{−2} day^{−1}) and the Barents Sea (>12 mmol m^{−2} day^{−1}) because of strong winds, and strongest in summer in the Chukchi Sea (~10 mmol m^{−2} day^{−1}) because of the sea-ice retreat. In recent years, the CO₂ uptake has increased in the Greenland/Norwegian Sea and decreased in the southern Barents Sea, owing to increased and decreased air–sea pCO₂ differences, respectively.

© 2016 The Authors. Published by Elsevier B.V. This is an open access article under the CC BY-NC-ND license (<http://creativecommons.org/licenses/by-nc-nd/4.0/>).

1. Introduction

Atmospheric CO₂ concentrations have increased since the 19th century, mainly because of fossil fuel burning, cement production, and land-use changes (Ciais et al., 2013). About half of the

emissions remain in the atmosphere, and the rest are stored in the oceans and terrestrial biosphere (Ciais et al., 2013). The contemporary net global uptake of CO₂ by the ocean has been estimated to be about 1.5 ± 0.5 PgC yr^{−1} (Gruber et al., 2009; Wanninkhof et al., 2013; Landschützer et al., 2014).

The Arctic Ocean and its adjacent seas (Fig. 1) are thought to act as a sink for atmospheric CO₂ because of the high solubility of CO₂ in its low-temperature waters (Bates and Mathis, 2009).

* Corresponding author. 2-15 Natsushima, Yokosuka, Kanagawa, 237-0061, Japan.
E-mail address: yasunaka@jamstec.go.jp (S. Yasunaka).

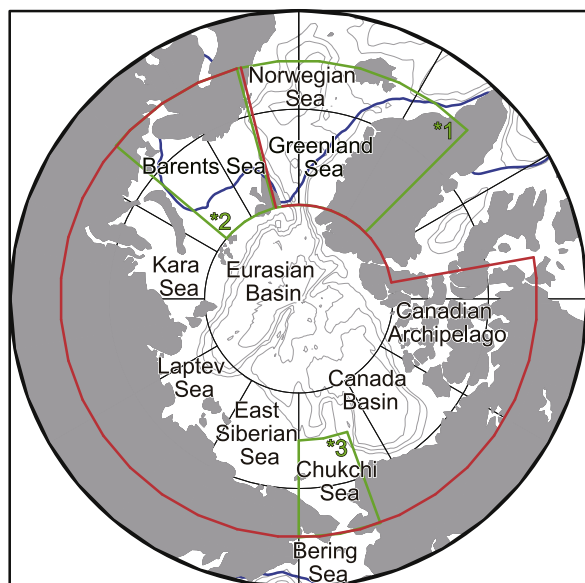


Fig. 1. Schematic map of the Arctic Ocean and its adjacent seas. Gray contours show the 1000, 2000, 3000, and 4000 m isobaths. Blue lines show the 17-year annual mean position of the ice edge (SIC = 15%). Sectors selected for the regional analysis: Arctic Ocean (red), Greenland/Norwegian Seas (green 1), Barents Sea (green 2), and Chukchi Sea (green 3).

Furthermore, as global warming progresses, melting of sea ice will increase the area of open water in the Arctic, thus enhancing the potential for the oceanic uptake of CO_2 from the atmosphere (e.g., Bates et al., 2006; Gao et al., 2012). It has been suggested, however, that the CO_2 uptake capacity has decreased in the Canada Basin (Cai et al., 2010; Else et al., 2013). Moreover, observational and model-based air–sea CO_2 fluxes in the Arctic show poor agreement in terms of seasonal cycles and interannual variability (Schuster et al., 2013), not only reflecting issues with the models but also large uncertainties in current, observational data-based estimates of the Arctic air–sea CO_2 flux (Bates and Mathis, 2009) because of the sparseness of CO_2 measurements in this very heterogeneous area (Fig. 2).

Several studies have attempted to address this situation by using other, more extensively observed seawater properties as proxies for the partial pressure of CO_2 in the surface water ($p\text{CO}_{2w}$) in this region utilizing multiple or simple linear regression techniques (e.g., Olsen et al., 2003; Nakaoka et al., 2006; Arrigo et al., 2010; Lauvset et al., 2013). However, the complex relationships between $p\text{CO}_{2w}$ and seawater properties and their domain and time dependence make regression-based approaches problematic (Lefèvre et al., 2005). As an alternative, a self-organizing map (SOM) technique has been implemented to estimate the $p\text{CO}_{2w}$ distribution from seawater properties in the North Atlantic and North Pacific (Telszewski et al., 2009; Nakaoka et al., 2013). The advantage of the SOM technique is its ability to empirically determine relationships among parameters without making any of the a priori assumptions of regression functions and without the need to divide the basin into sub-regions (Lefèvre et al., 2005; Telszewski et al., 2009). This is highly beneficial for applications to the Arctic, which includes continental shelves, central basins, and sea-ice-covered areas (Fig. 1) where the $p\text{CO}_{2w}$ distribution is affected by processes such as ocean heat loss and gain, sea-ice formation and melting, river discharge, shelf–basin interactions, and biological production and respiration (cf. Bates and Mathis, 2009). Furthermore, the SOM technique better reproduces the distribution of $p\text{CO}_{2w}$ from unevenly distributed observations than do multiple

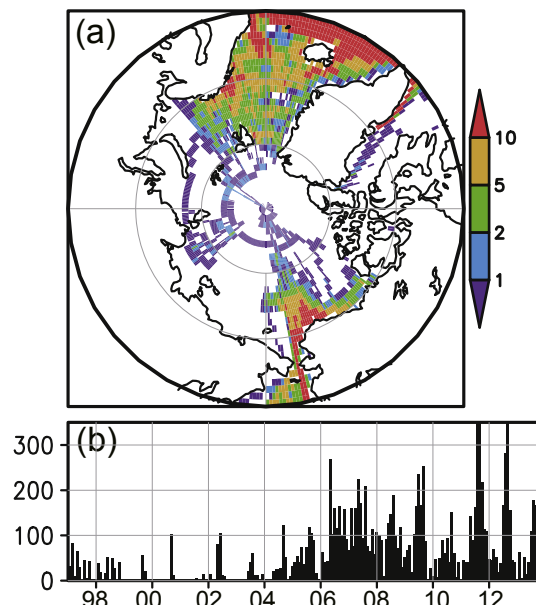


Fig. 2. (a) Grid boxes ($1^\circ \times 1^\circ$) in which at least one ocean surface CO_2 measurement was included in the SOCAT, LDEO, GLODAP, or CARINA databases, or obtained by R/V *Mirai* between 1997 and 2013. The colour scale indicates the number of months with available measurements among the 204 months during 1997–2013. (b) Monthly time series of the number of grid boxes with at least one ocean surface CO_2 measurement in the analysis area. (For interpretation of the references to colour in this figure legend, the reader is referred to the web version of this article.)

regression methods (Lefèvre et al., 2005). Therefore, we expected the SOM technique to be a useful tool for estimating $p\text{CO}_{2w}$ distributions in the Arctic.

In the present study, we created 204 monthly air–sea CO_2 flux maps of the Arctic north of 60°N , including the Arctic Ocean and its adjacent seas, with 1° (latitude) \times 1° (longitude) resolution for January 1997 to December 2013. To estimate the $p\text{CO}_{2w}$ distributions, we used a SOM trained with sea surface temperature (SST), sea surface salinity (SSS), sea-ice concentration (percentage of ocean area covered by sea ice, SIC), and atmospheric CO_2 mole fraction ($x\text{CO}_{2a}$) data. The mapping results were then used to investigate the basin-wide distribution and seasonal to interannual variability of air–sea CO_2 fluxes.

2. Data

2.1. $p\text{CO}_2$ measurements

We used $p\text{CO}_{2w}$ observations (converted from the fugacity of CO_2 values) from the Surface Ocean CO_2 Atlas (SOCAT) version 3 (Pfeil et al., 2013; Bakker et al., 2014, 2016; <http://www.socat.info/>), and the Global surface $p\text{CO}_2$ (LDEO) database version 2014 (Takahashi et al., 2015; http://cdiac.ornl.gov/oceans/LDEO_Underway_Database/). Duplicates between the SOCAT and LDEO databases were eliminated. We also used shipboard $p\text{CO}_{2w}$ measurements obtained during cruises of the R/V *Mirai* of the Japan Agency for Marine–Earth Science and Technology (JAMSTEC) that have not yet been archived in the SOCAT and LDEO databases (cruises MR09_03, MR10_05, MR12_E03, and MR13_06; <http://www.godac.jamstec.go.jp/darwin/e>). In total, we used 1,640,951 $p\text{CO}_{2w}$ measurements.

To improve the data coverage, we also used 1114 $p\text{CO}_{2w}$ data calculated from dissolved inorganic carbon and total alkalinity data in the Carbon Dioxide in the Atlantic Ocean (CARINA) database v1.2 (Tanhua et al., 2009; Key et al., 2010; Jutterström et al., 2010; <http://>

cdiac.ornl.gov/oceans/CARINA/) and in the Global Ocean Data Analysis Project (GLODAP) database (Key et al., 2004; <http://cdiac.ornl.gov/oceans/glodap/>), as well as dissolved inorganic carbon and total alkalinity data measured and compiled by scientists at the Institute of Ocean Sciences, Canada (Giesbrecht et al., 2013; now available as part of GLODAP version 2 database <http://cdiac.ornl.gov/oceans/GLODAPv2/>). We extracted values of samples obtained from water depths shallower than 10 m, or the shallowest values from the upper 30 m of each cast if there were no values from above 10 m. We used the CO2SYS program (Lewis and Wallace, 1998; van Heuven et al., 2009) and the dissociation constants reported by Lueker et al. (2000) and Dickson (1990) to calculate $p\text{CO}_{2w}$ from the dissolved inorganic carbon and total alkalinity data.

2.2. Gridded data sets

We used gridded datasets of SST, SSS, SIC, and $x\text{CO}_{2a}$ to train the SOM. The SST data were extracted from U.S. National Oceanic and Atmospheric Administration (NOAA) optimum interpolation SST version 2, which has a $1^\circ \times 1^\circ$ (latitude \times longitude) spatial and a monthly temporal resolution (Reynolds et al., 2002; <http://www.esrl.noaa.gov/psd/data/gridded/data.noaa.oisst.v2.html>). The SSS data were retrieved from the Polar Science Center Hydrographic Climatology version 3.0, which also has a $1^\circ \times 1^\circ$ spatial and a monthly temporal resolution (Steele et al., 2001; http://psc.apl.washington.edu/nonwp_projects/PHC/Climatology.html). The SIC data were obtained from the NOAA/National Snow and Ice Data Center Climate Data Record of Passive Microwave Sea Ice Concentration version 2, which has a spatial resolution of $25 \text{ km} \times 25 \text{ km}$ and a monthly temporal resolution (Meier et al., 2013; <http://nsidc.org/data/G02202>). These data were subsequently averaged into $1^\circ \times 1^\circ$ monthly grids by us. Finally, zonal mean $x\text{CO}_{2a}$ data were retrieved from the NOAA Greenhouse Gas Marine Boundary Layer Reference data product (Conway et al., 1994; <http://www.esrl.noaa.gov/gmd/ccgg/mbi/index.html>); we also interpolated these data into $1^\circ \times 1^\circ$ monthly grids.

3. $p\text{CO}_2$ mapping and calculation of fluxes

3.1. Gridding procedure for CO_2 measurements

We gridded the individual $p\text{CO}_{2w}$ measurements from 1997 to 2013 into a $1^\circ \times 1^\circ$ spatial grid with a monthly temporal resolution to match the resolution of the data used to train the SOM. First, we calculated the long-term mean (i.e., the climatology) and its standard deviation in a window size of ± 2 months, $\pm 5^\circ$ of latitude, and $\pm 30^\circ$ of longitude for each $1^\circ \times 1^\circ$ monthly grid. We then eliminated data that differed by more than three standard deviations from the climatology. Next, we recalculated the climatology and its standard deviation in a smaller window size of ± 1 month, $\pm 2^\circ$ of latitude, and $\pm 10^\circ$ of longitude for each $1^\circ \times 1^\circ$ monthly grid, and again eliminated extreme data that differed from the climatology by more than three standard deviations of the climatology. In the end, we excluded about 0.5% of all measurements as extreme or erroneous data; these excluded data were randomly distributed in time and space. Finally, we binned the remaining measurements into $1^\circ \times 1^\circ$ monthly grid boxes for each year from 1997 to 2013 (Fig. 2). Most of the available data were from the Greenland, Norwegian, Barents, and Chukchi Seas; there were no measurements from the East Siberian Sea. CO_2 measurements were available for almost all seasons of 1997 and 1998 and after 2004, but only for summer during the period from 1999 to 2003. Although some studies have used $p\text{CO}_{2w}$ normalized to a certain year (e.g., Takahashi et al., 2009), we used the measured (“non-normalized”) $p\text{CO}_{2w}$ values; therefore, $p\text{CO}_{2w}$ could increase both non-linearly in time and non-uniformly in space.

3.2. $p\text{CO}_2$ estimation using a self-organizing map

We estimated $p\text{CO}_{2w}$ by a SOM technique similar to that used by Telszewski et al. (2009) and Nakaoka et al. (2013). In our estimation, we used SST, SSS, SIC, and $x\text{CO}_{2a}$ as training parameters. Among those variables representing the spatial distribution and temporal variation of surface water properties in the Arctic, SST, SSS, and SIC are basic parameters and their gridded products are readily available. They also closely relate to processes causing variation in $p\text{CO}_{2w}$: SST relates directly to the temperature dependency of $p\text{CO}_{2w}$; SSS represents the freshwater effect on $p\text{CO}_{2w}$; and SIC reflects the magnitude of the sea-ice barrier to air–sea CO_2 exchange. $x\text{CO}_{2a}$ represents atmospheric CO_2 seasonal variations and its long-term increase. Because we used non-normalized $p\text{CO}_{2w}$ values, $x\text{CO}_{2a}$ also serves as a time indicator. However, $p\text{CO}_{2w}$ distributions estimated by using only these four parameters included high and low values intricately intermingled in space and time in regions and seasons with limited CO_2 observations (not shown). To deal with this situation, which means some physical or chemical parameters would be missing, we added geographical position to the set of training parameters: $X = \sin(\text{latitude}) \times \cos(\text{longitude})$ and $Y = \sin(\text{latitude}) \times \sin(\text{longitude})$. The use of geographical position as a training parameter can prevent a systematic spatial bias (Yasunaka et al., 2014), although it degrades the results in some cases (Telszewski et al., 2009). Previous studies have used mixed layer depth and chlorophyll-*a* concentration as training parameters to account for vertical mixing and biological effects, respectively, but we did not use these parameters because of insufficient data coverage in the Arctic.

We estimated the basin-wide $p\text{CO}_{2w}$ fields by a three-step SOM technique. Telszewski et al. (2009) and Nakaoka et al. (2013) describe the technique in detail, so we outline only the basic principles here. First, the about a million $1^\circ \times 1^\circ$ monthly pixels in the analysis region and period were assigned to 5000 units (neurons) on the SOM by using the SST, SSS, SIC, $x\text{CO}_{2a}$, and X and Y data; this is the training of the SOM. Second, each neuron was labeled with the $p\text{CO}_{2w}$ value observed at the pixel at which SST, SSS, SIC, $x\text{CO}_{2a}$, and X and Y values were most similar to those of the neuron. Third, each pixel in the analysis region and period was assigned to the $p\text{CO}_{2w}$ value of the neuron whose SST, SSS, SIC, $x\text{CO}_{2a}$, and X and Y values were most similar to the values at that pixel. If the most similar neuron was not labeled with a $p\text{CO}_{2w}$ value, then the $p\text{CO}_{2w}$ value of the neuron that was most similar and labeled was used. Thus, by using the SOM technique, we were able to estimate $p\text{CO}_{2w}$ values even in regions and periods with no CO_2 observations.

3.3. Calculation of air–sea CO_2 fluxes

We calculated monthly air–sea CO_2 flux (F) values from the $p\text{CO}_{2w}$ values estimated as described in section 3.2 by using the bulk formula of Wanninkhof (1992):

$$F = kL(p\text{CO}_{2w} - p\text{CO}_{2a}) \quad (1)$$

where k is the gas transfer velocity and L is the solubility of CO_2 . The solubility of CO_2 was calculated as a function of temperature and salinity (Weiss, 1974). We converted NOAA $x\text{CO}_{2a}$ data to $p\text{CO}_{2a}$ data by using monthly sea level pressure data from the U.S. National Centers for Environmental Prediction–Department of Energy Reanalysis 2 (NCEP 2) (Kanamitsu et al., 2002; <http://www.esrl.noaa.gov/psd/data/gridded/data.ncep.reanalysis2.html>) and the water vapor saturation pressure calculated from monthly SST (Murray, 1967).

We used the monthly average of the 6-hourly 10-m wind speeds from NCEP 2. Therefore, we adjusted the gas exchange coefficient to

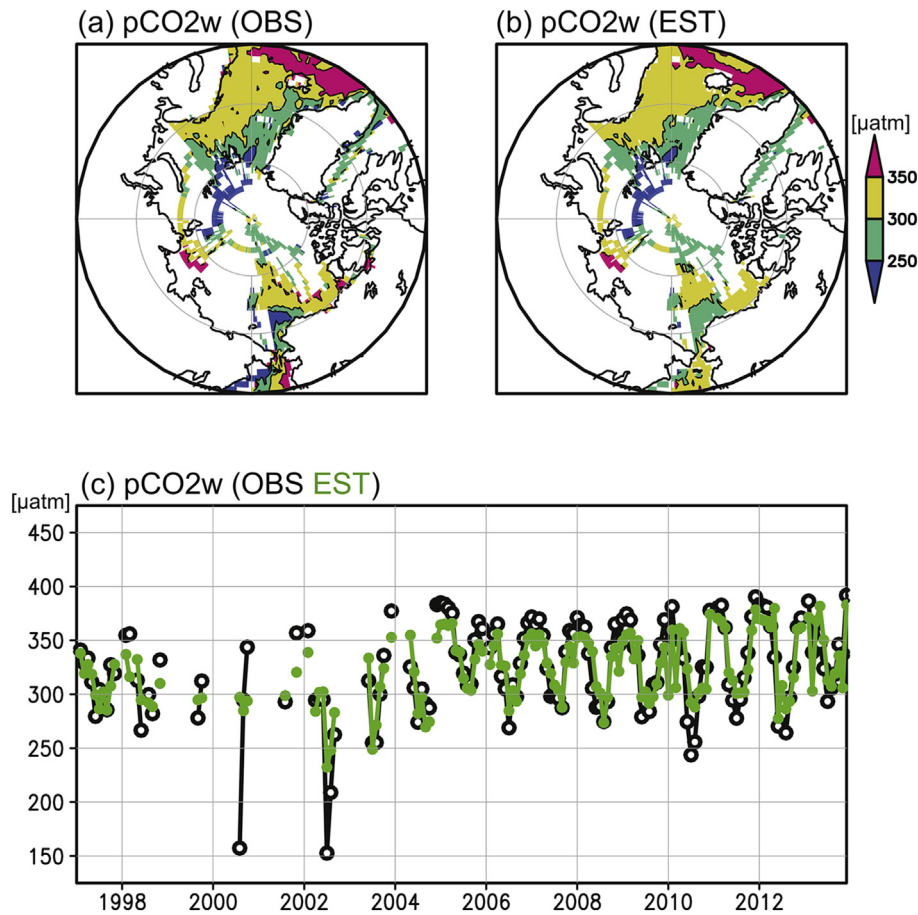


Fig. 3. (a) Observed $p\text{CO}_{2w}$ averaged over the whole analysis period [μatm]. (b) Estimated $p\text{CO}_{2w}$ averaged over the grid boxes in which observed $p\text{CO}_{2w}$ values were available [μatm]. (c) Monthly time series of observed $p\text{CO}_{2w}$ averaged over the entire analysis area (black), and estimated $p\text{CO}_{2w}$ averaged over the grid boxes in which observed $p\text{CO}_{2w}$ values were available (green) [μatm]. (For interpretation of the references to colour in this figure legend, the reader is referred to the web version of this article.)

that of Sweeney et al. (2007), using the same method as Schuster et al. (2013) and Wanninkhof et al. (2013). To optimize the gas exchange coefficient for NCEP 2 winds, instead of the NCEP 1 winds used by Sweeney et al. (2007), we calculated the global annual average of $0.27\langle W_{\text{NCEP1}}^2 \rangle / \langle W_{\text{NCEP2}}^2 \rangle$, where 0.27 is the original gas

exchange coefficient of Sweeney et al. (2007) and $\langle W^2 \rangle$ is the monthly mean of the 6-hourly wind second moment, and obtained a value of 0.19. Thus,

$$k = 0.19(\text{Sc}/660)^{-0.5} \langle W_{\text{NCEP2}}^2 \rangle \quad (2)$$

where Sc is the Schmidt number of CO_2 in seawater at a given SST. The relationship between Sc and SST in seawater is given by Wanninkhof (2014).

The suppression effect of sea ice on gas exchange was accounted for by correcting the air–sea CO_2 fluxes using the parameterization suggested by Loose et al. (2009), where the flux is proportional to (ice-free proportion)^{0.4}. In this parameterization, the flux in the sea ice region was larger than the value would be if it were determined by assuming a linear relationship with the open-water area, because circulation under the ice affects the gas exchange rate. Following Bates et al. (2006), in those regions with >99% SIC, we used 99% SIC to allow for non-negligible rates of air–sea CO_2 exchange through leads, fractures, and brine channels (Semiletov et al., 2004).

3.4. Uncertainties of $p\text{CO}_2$ mapping and CO_2 flux estimation

Our $p\text{CO}_{2w}$ estimates reproduced the general features of the spatial distribution and temporal variation of the observed data (Fig. 3; Note that the spatial and temporal changes depicted in Fig. 3 include differences in the observed seasons and changes in the

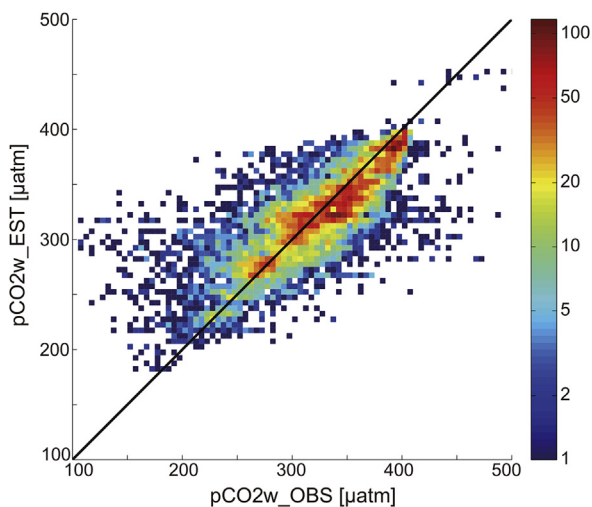


Fig. 4. Scatter plot of estimated $p\text{CO}_{2w}$ versus observed $p\text{CO}_{2w}$. Colors indicate the number of data pairs in a $5 \mu\text{atm} \times 5 \mu\text{atm}$ bin.

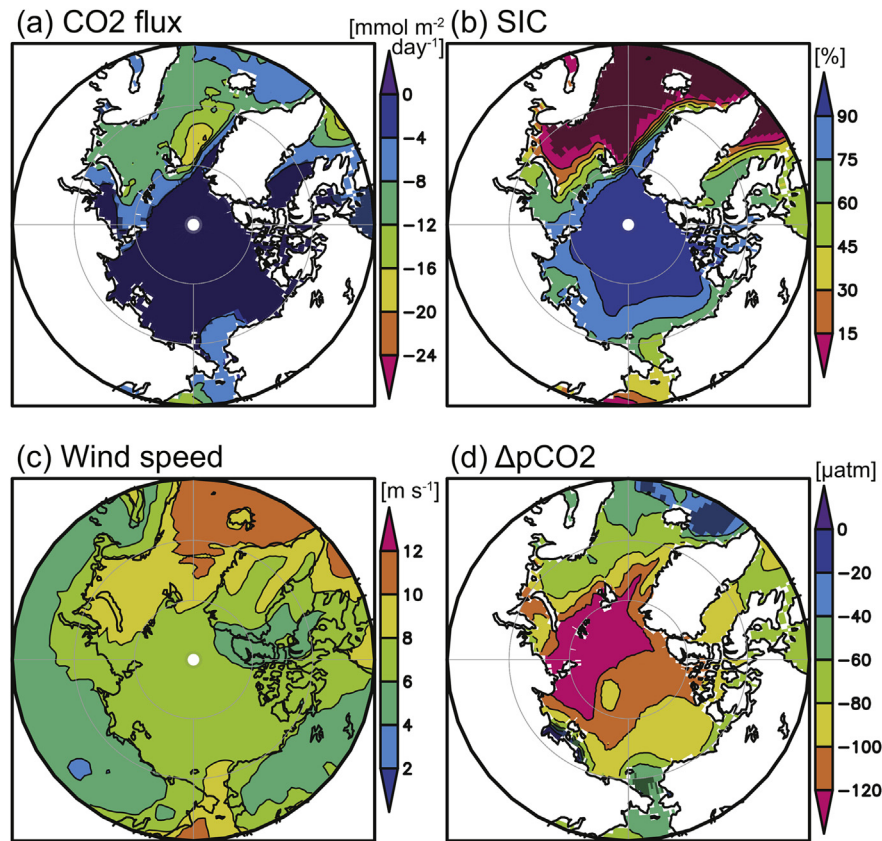


Fig. 5. Seventeen-year annual means of (a) CO₂ flux [$\text{mmol m}^{-2} \text{day}^{-1}$] (negative values indicate influx into the ocean), (b) SIC [%], (c) wind speed [m s^{-1}], and (d) $\Delta p\text{CO}_2$ ($= p\text{CO}_{2w} - p\text{CO}_{2a}$) [μatm]. Darker shades show values in grids where values were smaller than the uncertainty.

Table 1

Comparison of annual mean CO₂ fluxes [$\text{mmol m}^{-2} \text{day}^{-1}$] averaged in the Greenland/Norwegian, Barents, and Chukchi Seas, and the Arctic Ocean between this study and previous studies (negative values indicate influx into the ocean).

Area	CO ₂ flux	Method of $p\text{CO}_{2w}$ estimate	Reference
Greenland/Norwegian Seas	-11 ± 3	SOM technique	This study
	-12 ± 1	Observation	Anderson et al. (2000)
	-10	Interpolation	Takahashi et al. (2009)
	-8 ± 3	Interpolation	Land et al. (2013)
	-12 ± 5	Multiple linear regression	Nakaoka et al. (2006)
	-9	Multiple linear regression	Arrigo et al. (2010)
Barents Sea	-2	Biogeochemical Model	Manizza et al. (2013)
	-10 ± 4	SOM technique	This study
	-10 ± 2	Carbon balance	Fransson et al. (2001)
	-7 ± 3	Carbon balance	Kaltin et al. (2002)
	-4	Interpolation	Takahashi et al. (2009)
	-2 ± 1	Interpolation	Land et al. (2013)
Chukchi Sea	-11 ± 4	Multiple linear regression	Nakaoka et al. (2006)
	-12 ± 2	Multiple linear regression	Omar et al. (2007)
	-4	Multiple linear regression	Arrigo et al. (2010)
	-11 ± 1	Multiple linear regression	Lauvset et al. (2013)
	-4	Biogeochemical Model	Manizza et al. (2013)
	-4 ± 4	SOM technique	This study
Arctic Ocean	-14 ± 2	Observation	Bates et al. (2006)
	-4 ± 2	Observation	Evans et al. (2015)
	-20 ± 5	Carbon balance	Kaltin and Anderson (2005)
	-1	Interpolation	Takahashi et al. (2009)
	-1	Biogeochemical Model	Manizza et al. (2013)
	-4 ± 4	SOM technique	This study
	-1.7 to -4.2	Integration of many studies	Bates and Mathis (2009)

positions of the observation points). Both observed and estimated $p\text{CO}_{2w}$ tended to be lower in the Greenland, Barents, and Chukchi Seas than in the Norwegian Sea or the shelf region between the

Chukchi Sea and the Canada Basin. However, the north–south contrast in the Chukchi Sea and the east–west contrast in the Bering Sea in our estimates were weaker than those in the

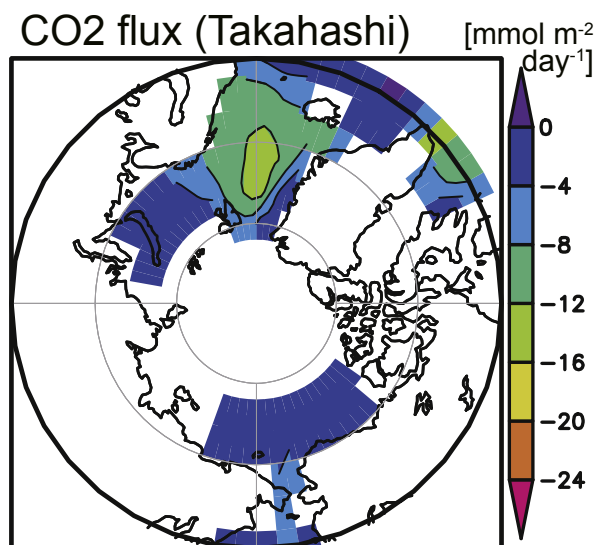


Fig. 6. Annual mean climatology of the CO₂ flux [mmol m⁻² day⁻¹] from the data of Takahashi et al. (2009) (http://www.ideo.columbia.edu/res/pi/CO2/carbondioxide/air_sea_flux/sumflux_2006c.txt).

observations (see also Fig. S1a); we attribute these weaker contrasts to the fact that our estimates did not fully represent the low $p\text{CO}_{2w}$ values accompanying high primary production in waters originating in the Pacific (Bates et al., 2006). The temporal changes in the observed and estimated $p\text{CO}_{2w}$ were in phase, although the variability of the estimated values was somewhat subdued compared to that of the observed data (see also Fig. S1c).

In a scatter plot of estimated versus observed $p\text{CO}_{2w}$ values, the data points cluster around the 1:1 line (Fig. 4). The correlation coefficient between estimated and observed $p\text{CO}_{2w}$ values was 0.80, and the root mean squared difference (RMSD) was 32 μatm , or 10% of the average observed $p\text{CO}_{2w}$ value. The RMSD between observed and estimated $p\text{CO}_{2w}$ was large in the Chukchi and Bering Seas (Fig. S1b). The observed $p\text{CO}_{2w}$ values included uncertainties that did not exceed the difference between the estimated and observed values as follows: The uncertainty of the $p\text{CO}_{2w}$ measurements is 2–5 μatm (Bakker et al., 2014). If the uncertainties of dissolved inorganic carbon and alkalinity are within 4 $\mu\text{mol kg}^{-1}$ and 6 $\mu\text{mol kg}^{-1}$, respectively (Key et al., 2004; Jutterström et al., 2010; Giesbrecht et al., 2013), then the uncertainty of the calculated $p\text{CO}_{2w}$ values can be up to 14 μatm (Lueker et al., 2000). The sampling uncertainty of the gridded $p\text{CO}_{2w}$ observation data was deduced from the standard errors of monthly observed $p\text{CO}_{2w}$ in the $1^\circ \times 1^\circ$ grid to be 7 μatm . Like the RMSD, the sampling uncertainty also tended to be large in the Chukchi and Bering Seas (not shown).

To validate our estimated $p\text{CO}_{2w}$ values for periods and regions without any observed data, we systematically excluded some of the observed $p\text{CO}_{2w}$ data when labeling neurons, then redid the mapping and evaluated how well the SOM technique was able to estimate the excluded data. We carried out four experiments by excluding data (1) for 1997–2004, (2) for January to April, (3) from north of 80°N , and (4) from the Laptev Sea ($90^\circ\text{E} - 150^\circ\text{E}$), where there were only a few $p\text{CO}_{2w}$ observations. We compared the $p\text{CO}_{2w}$ estimates obtained in each experiment with the excluded observations and found that the $p\text{CO}_{2w}$ estimates reproduced the general features of the observed spatial distribution and temporal variation, and they were also similar to the $p\text{CO}_{2w}$ estimates obtained by using all observations (Figs. S2–S5). However, the RMSDs between the estimates and the excluded observations were about $1\frac{1}{2}$ – $2\frac{1}{2}$

times (1.9 times on average) larger than the RMSDs of the estimates based on all observations. This result suggests that the uncertainty in $p\text{CO}_{2w}$ might be as high as 61 μatm in regions and periods without data. We used this uncertainty for $p\text{CO}_{2w}$ estimates made by using the values of a less similar neuron.

Signorini and McClain (2009) estimated the uncertainty of the CO₂ flux derived from the gas exchange parameterization to be 36%, and that derived from the wind data to be 11%. We used an uncertainty of 5% for SIC (Cavaliere et al., 1984; Gloersen et al., 1993; Peng et al., 2013). The standard error of the SIC effect on gas exchange is about 30% (Loose et al., 2009). The uncertainty of $p\text{CO}_{2a}$ is about 0.5 μatm ($\ll 1\%$; <http://www.esrl.noaa.gov/gmd/ccgg/mb/mb.html>), and that of $p\text{CO}_{2w}$ is 32 μatm ; therefore, we estimated the uncertainty of $\Delta p\text{CO}_2$ ($= p\text{CO}_{2w} - p\text{CO}_{2a}$) to be 36% (average $\Delta p\text{CO}_2$ in the analysis domain and period was $-89 \mu\text{atm}$). Thus, we estimated the overall uncertainty of the estimated CO₂ fluxes to be 60% $[(0.36^2 + 0.11^2 + 0.05^2 + 0.3^2 + 0.36^2)^{1/2}]$. In regions and periods without any observed data, we used an uncertainty of 83% $[(0.36^2 + 0.11^2 + 0.05^2 + 0.3^2 + 0.68^2)^{1/2}]$, because in those regions the uncertainty of the $\Delta p\text{CO}_2$ estimates could be as high as 68%. Because the average of the estimated CO₂ flux in the analysis domain and period was 5.6 mmol m⁻² day⁻¹, the uncertainty of the CO₂ flux estimate was 3.4 mmol m⁻² day⁻¹, but in regions and periods without observed data, it was 4.6 mmol m⁻² day⁻¹. Some part of the uncertainty consists of random error and would be reduced by averaging, but it is difficult to quantitatively separate the uncertainty due to random error from that due to systematic error; therefore, in every case we used 3.4 mmol m⁻² day⁻¹ and 4.6 mmol m⁻² day⁻¹ as the upper limits of the uncertainty. Our uncertainties tended to be large because we included not only the uncertainties of the $p\text{CO}_{2w}$ estimate, wind speed data, and the gas exchange parameterization, as other studies have (e.g., Arrigo et al., 2010; Land et al., 2013), but also those of the SIC effect and of $p\text{CO}_{2w}$ estimation in periods and regions without observations, which have not been considered by other studies.

4. Spatiotemporal CO₂ flux variability

4.1. Seventeen-year annual mean state

The 17-year annual mean CO₂ flux distribution shows that all areas of the Arctic Ocean and its adjacent seas were net CO₂ sinks (Fig. 5a). The annual CO₂ influx to the ocean was strong in the Greenland/Norwegian Seas ($>10 \text{ mmol m}^{-2} \text{ day}^{-1}$), the Barents Sea ($\sim 10 \text{ mmol m}^{-2} \text{ day}^{-1}$), and the Chukchi Sea ($\sim 4 \text{ mmol m}^{-2} \text{ day}^{-1}$). In contrast, it was weak within the uncertainty in the Eurasian and Canada Basins, as well as in the Laptev and East Siberian Seas ($<4 \text{ mmol m}^{-2} \text{ day}^{-1}$). Our annual CO₂ flux estimates averaged in the Greenland/Norwegian Seas and the Barents Sea are consistent with those reported by most previous studies (Table 1). Our estimate of the average CO₂ influx in the Chukchi Sea was smaller than that based on observations by Bates et al. (2006), but consistent with a recent observation-based estimate by Evans et al. (2015). CO₂ fluxes reported by Takahashi et al. (2009) show influxes of similar magnitude to ours in the Greenland/Norwegian Seas and the Chukchi Sea, but a smaller influx in the Barents Sea (Fig. 6). The contrast between large and small fluxes in the Greenland Sea was sharper in our estimates than that in the study by Takahashi et al. (2009). Estimates of CO₂ influxes into the Arctic Ocean produced by a biogeochemical model (Manizza et al., 2013) are weaker than most other estimates, including ours.

Next, we examine the relationship between the CO₂ flux and SIC, wind speed, and $\Delta p\text{CO}_2$, parameters that directly relate to the CO₂ flux. The annual mean CO₂ flux distribution showed strong similarities to the SIC and wind distributions (Fig. 5b and c). The 75% SIC

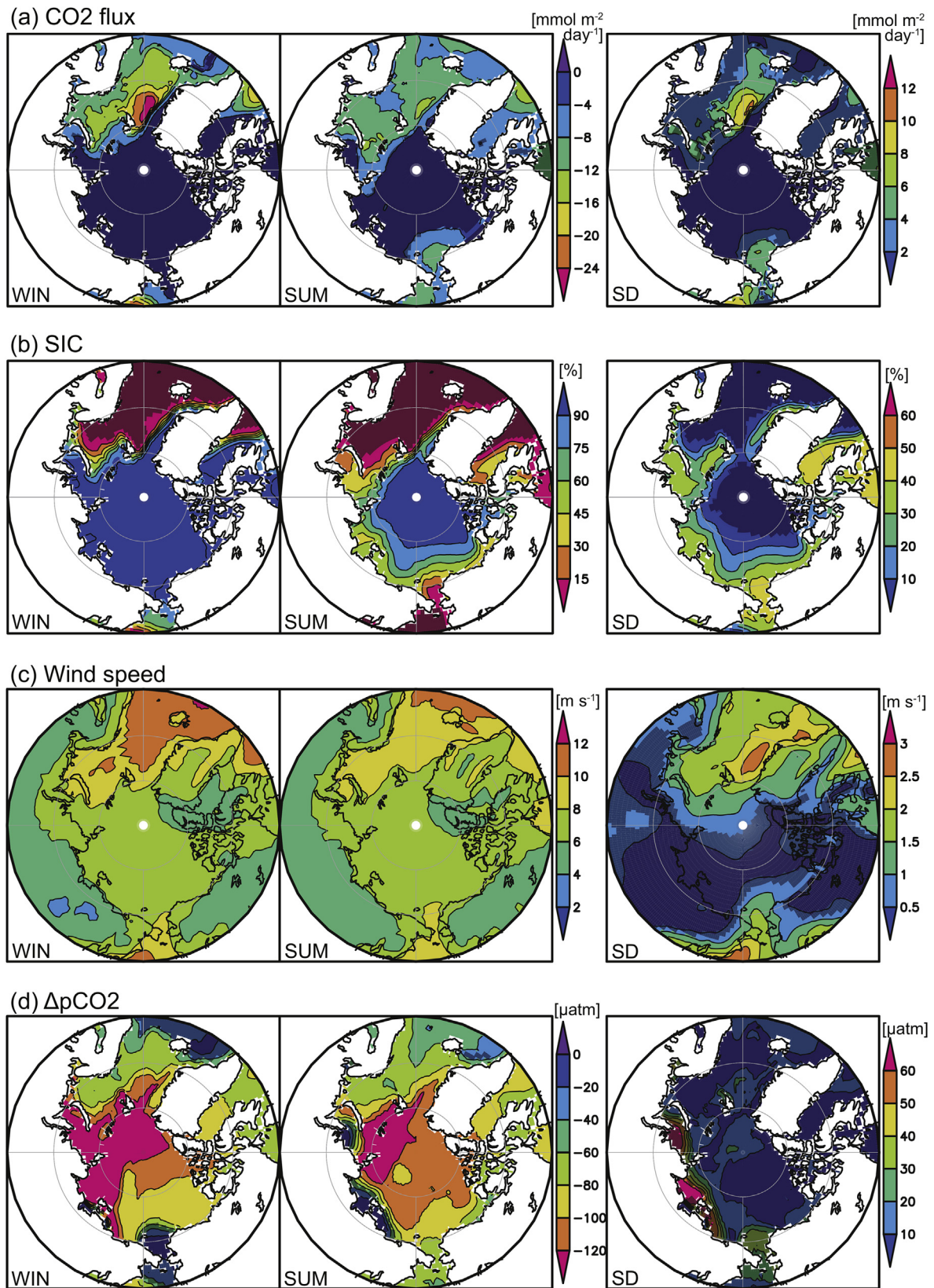


Fig. 7. (a) CO₂ flux [mmol m⁻² day⁻¹], (b) SIC [%], (c) wind speed [m s⁻¹], and (d) ΔpCO₂ [μatm] averaged from December to May (left) and from June to November (middle), and standard deviations calculated from 17-year monthly means (right). Darker shades show values in grids where values were smaller than the uncertainty.

contour mostly corresponds to the $-4 \text{ mmol m}^{-2} \text{ day}^{-1}$ contour of the CO₂ flux, indicating that in the area with an average sea-ice

cover of more than 75%, the CO₂ influx was less than $4 \text{ mmol m}^{-2} \text{ day}^{-1}$. Strong fluxes into the Greenland/Norwegian

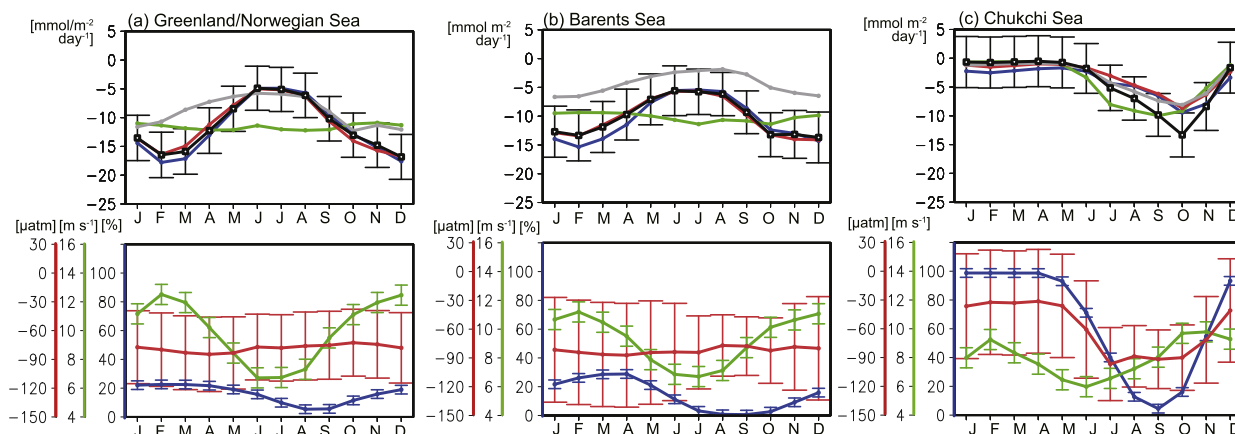


Fig. 8. Area-mean seasonal variations in (a) the Greenland/Norwegian Seas (65°–80°N, 45°W–15°E), (b) the Barents Sea (65°–80°N, 15°–50°E), and (c) the Chukchi Sea (65°–75°N, 180°–160°W). The upper panels show seasonal variations in the CO₂ flux (black, standard; blue, SIC constant; green, wind constant; red, ΔpCO₂ constant; gray, from Takahashi et al., 2009) in each region [mmol m⁻² day⁻¹], and the lower panels show seasonal variations in SIC [%] (blue), wind speed [m s⁻¹] (green), and ΔpCO₂ [μatm] (red). Error bars indicate the uncertainty. (For interpretation of the references to colour in this figure legend, the reader is referred to the web version of this article.)

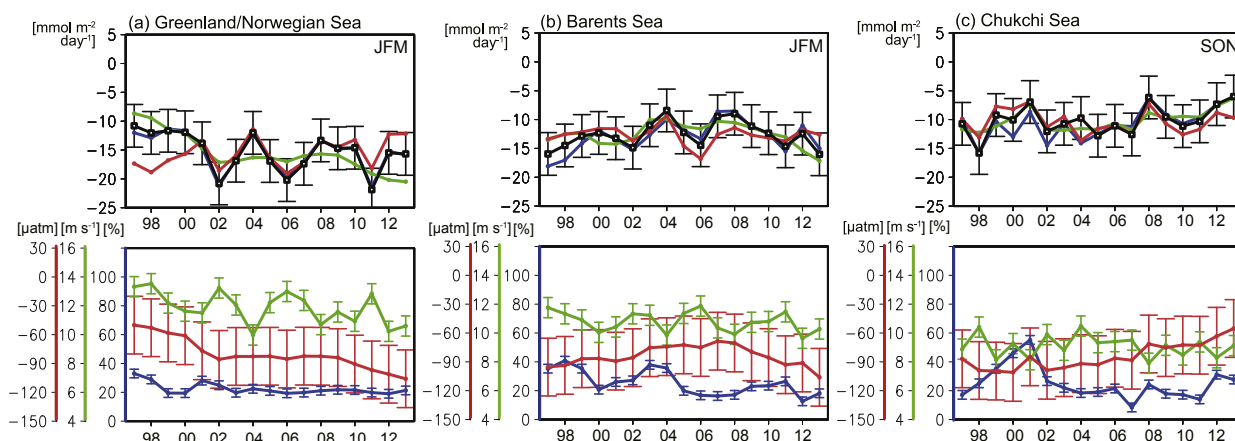


Fig. 9. Area-mean interannual variations in (a) the Greenland/Norwegian Seas and (b) the Barents Sea from January to March, and (c) the Chukchi Sea from September to November. The upper panels show interannual variations in the CO₂ flux (black, standard; blue, SIC constant; green, wind constant; red, ΔpCO₂ constant) in each region [mmol m⁻² day⁻¹], and the lower panels show interannual variations in SIC [%] (blue), wind speed [m s⁻¹] (green), and ΔpCO₂ [μatm] (red). Error bars indicate the uncertainty. (For interpretation of the references to colour in this figure legend, the reader is referred to the web version of this article.)

Seas, the Barents Sea, and the Chukchi Sea were associated with high winds and large areas of open water in those regions. In the Eurasian Basin, the CO₂ influx was relatively small because of the large SIC (>75%), even though ΔpCO₂ was highly negative (Fig. 5d).

If, following Bates and Mathis (2009), we define the Arctic Ocean as the ocean area north of 65°N excluding the Greenland/Norwegian Seas and Baffin Bay (outlined in red in Fig. 1; 10.7×10^6 km²), the estimated 17-year average influx to the Arctic Ocean is 4 mmol m⁻² day⁻¹, equivalent to an uptake of 180 TgC yr⁻¹. The formal uncertainty is large (210 TgC yr⁻¹), however, mainly because of the poor coverage of pCO₂ observations and the uncertainty of the SIC effect on gas exchange. Nevertheless, our estimate is consistent with the range of 81–199 TgC yr⁻¹ (uncertainty unspecified) reported by Bates and Mathis (2009) in their comprehensive review.

4.2. Seasonal variation

We calculated 17-year monthly mean CO₂ fluxes and related variables (Figs. 7 and 8). We considered December–May to be winter and June–November to be summer, defined on the basis of

the maximum SIC, which occurs in March, and the minimum SIC, which occurs in September. To examine the effects of wind speed, SIC, and ΔpCO₂ on the seasonal changes in the CO₂ flux, we recalculated the CO₂ fluxes by replacing each of these variables, one at a time, by a constant value (i.e., the 17-year annual mean; the upper panels of Fig. 8).

In winter, the CO₂ influx was strongest in the Greenland/Norwegian Seas (>15 mmol m⁻² day⁻¹) and the Barents Sea (>12 mmol m⁻² day⁻¹), and in summer it was strongest in the Chukchi Sea (~10 mmol m⁻² day⁻¹). The seasonal variation of the CO₂ flux was large in the Greenland/Norwegian Seas, the Chukchi Sea, and a part of the Barents Sea. Seasonal amplitudes were more than 10 mmol m⁻² day⁻¹ in the Greenland/Norwegian Seas and close to 10 mmol m⁻² day⁻¹ in the Barents and Chukchi Seas.

The seasonal variations of the CO₂ flux generally corresponded to wind speed and SIC variations. As with the 17-year annual mean, the seasonal CO₂ flux was weak in sea-ice-covered regions (e.g., the Eurasian Basin), but in regions where the SIC was less than ~50% (such as above the continental shelves), the seasonal variation of the CO₂ flux corresponded to the seasonal variation of wind speed. The seasonal variation of ΔpCO₂, however, was almost insignificant and

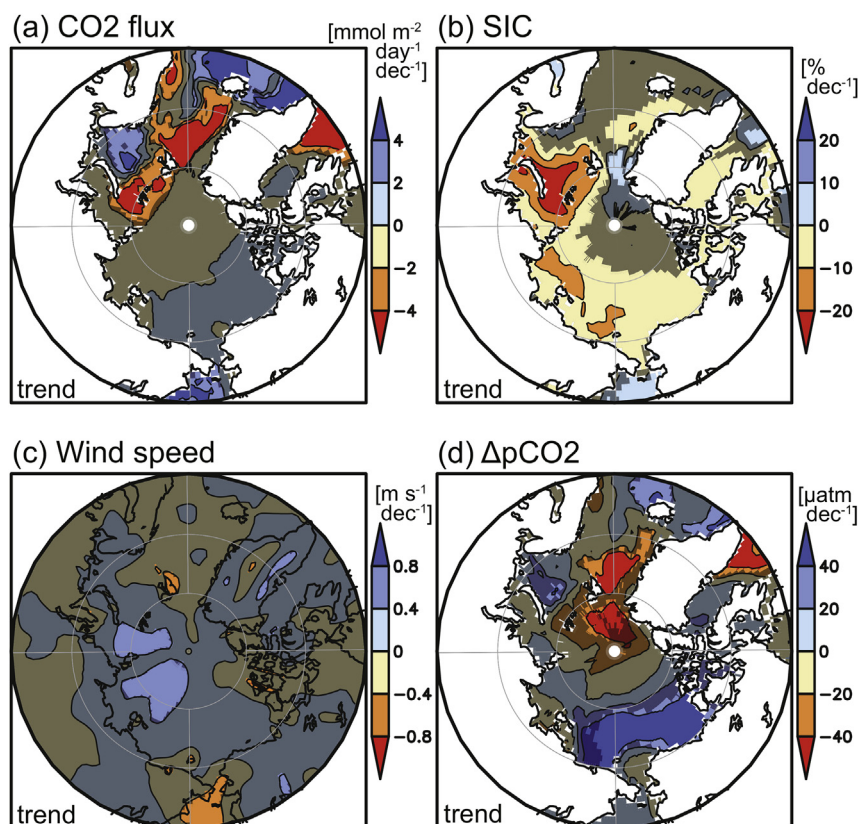


Fig. 10. Trends in (a) CO_2 flux [$\text{mmol m}^{-2} \text{day}^{-1} \text{decade}^{-1}$], (b) SIC [$\% \text{decade}^{-1}$], (c) wind speed [$\text{m s}^{-1} \text{decade}^{-1}$], and (d) $\Delta p\text{CO}_2$ [$\mu\text{atm decade}^{-1}$]. Darker shades show values in grids where values were smaller than the uncertainty.

had a limited impact on the CO_2 flux. As indicated by the reduction of the variance that occurred when each variable was replaced in turn with a constant value, wind speed explained 65%, SIC explained 22%, and $\Delta p\text{CO}_2$ explained 13% of the seasonal CO_2 flux changes averaged in the overall analysis area.

In the Chukchi Sea, which is seasonally covered with ice, the CO_2 flux was very small from December to May, and then after June, when SIC dropped to less than 80%, the CO_2 influx began to increase. It continued to increase as SIC decreased and the wind strengthened, reaching a maximum in October. The larger negative $\Delta p\text{CO}_2$ values from June to November in the Chukchi Sea can be attributed to the lowering of $p\text{CO}_{2w}$ as a result of biological CO_2 consumption (Bates et al., 2005) and the addition of sea-ice melt-water (Bates et al., 2014). Because biological production becomes high in the Chukchi Sea once sunlight reappears, followed by temperature increases and a sea-ice retreat (Cota et al., 1996), the training parameters SST and SIC probably function to some extent as proxies for the biological $p\text{CO}_{2w}$ drawdown.

The seasonal cycles of the CO_2 flux estimated here are consistent with those estimated by other regional studies. The seasonal cycles in the Greenland and Barents Seas are in phase with the estimates of Anderson et al. (2000), Nakaoka et al. (2006), Arrigo et al. (2010), and Land et al. (2013), although the seasonal amplitudes of our $p\text{CO}_{2w}$ and $\Delta p\text{CO}_2$ estimates were smaller than those of these other studies (but the discrepancy is smaller than the uncertainty of our estimate). The seasonal cycle in our estimate for the Chukchi Sea is consistent with the strengthening of the CO_2 influx from spring to early autumn in the observation-based studies by Murata and Takizawa (2003), Bates et al. (2006), and Evans et al. (2015). The seasonal cycles of the flux in the Greenland/Norwegian, Barents, and Chukchi Seas estimated in this study are also in phase with

those estimated by Takahashi et al. (2009), although our estimated amplitudes are larger (Fig. 8).

4.3. Interannual variation

Interannual variation of the CO_2 flux was larger than uncertainty in the Greenland/Norwegian Seas and the Barents Sea in early winter, and in the Chukchi Sea in late summer (Fig. 9). The amplitudes of the interannual variation in these regions were about $10 \text{ mmol m}^{-2} \text{day}^{-1}$. The CO_2 influx in the Greenland/Norwegian Seas and the Barents Sea was large in 2002, 2006, and 2011, mainly because of stronger winds in those years. The CO_2 influx in the Chukchi Sea was weak in 2001 and strong in 2007 because of SIC change. In contrast, the interannual variation of $\Delta p\text{CO}_2$ affected the interannual variation of the CO_2 flux at longer time scales. We calculated the overall contributions of SIC, wind speed, and $\Delta p\text{CO}_2$ to the interannual CO_2 flux variation by re-calculating the CO_2 fluxes after replacing each of these variables, one at a time, with the 17-year monthly mean value (See the upper panels of Fig. 9). The contributions of SIC, wind, and $\Delta p\text{CO}_2$ to the interannual CO_2 flux variation in the overall analysis area were 8%, 13%, and 79%, respectively. The $\Delta p\text{CO}_2$ contribution to the interannual variation was thus much larger than its contribution to the seasonal variation of the CO_2 fluxes. About 80% of the $\Delta p\text{CO}_2$ interannual variation arose from the interannual variation of $p\text{CO}_{2w}$.

The 17-year trend in the CO_2 flux was negative (i.e., uptake by the ocean was increasing) in the Greenland/Norwegian Seas and northern Barents Sea, and positive (i.e., uptake was decreasing) in the southern Barents Sea (Fig. 10). The 17-year trends were larger than the uncertainty in these regions. In the Greenland/Norwegian and Barents Seas, the spatial distribution of the CO_2 flux trend

corresponded well to that of the $\Delta p\text{CO}_2$ trend. The positive $\Delta p\text{CO}_2$ trend (i.e., decreased undersaturation of CO_2) in the southeastern Barents Sea was accompanied by decreasing SIC. A positive $\Delta p\text{CO}_2$ trend and decreasing SIC were also found in the Canada Basin, the East Siberian Sea, and the northern Chukchi Sea, although the CO_2 flux trend was small in those regions. The $\Delta p\text{CO}_2$ trend in all of these regions corresponded well to the SST trend (not shown). This result shows that whether $p\text{CO}_{2w}$ increased faster or slower than the increasing $p\text{CO}_{2a}$ depended on the thermodynamic relationships. Cai et al. (2010) also reported a rise in $p\text{CO}_{2w}$ with increasing SST in the Canada Basin. Simultaneous trends toward positive $\Delta p\text{CO}_2$ and decreased SIC suggest that the CO_2 uptake can be expected to decrease once the ocean becomes free of sea ice, as suggested by Cai et al. (2010). In the northern Barents Sea, however, the retreating sea ice increased the CO_2 influx into the sea, probably as a result of increased biological CO_2 consumption (i.e., primary production), which is attributable in turn to increased surface stratification caused by the addition of sea-ice meltwater (e.g., Fransson et al., 2001) and increased light availability. Retreating sea ice has two opposite effects on $p\text{CO}_{2w}$ and the CO_2 flux; on the one hand, it leads to increased $p\text{CO}_{2w}$ due to increased SST, while on the other hand, it leads to decreased $p\text{CO}_{2w}$ due to active biological production.

Our estimated interannual CO_2 flux changes in the Greenland and Barents Seas are consistent with the regression-based estimate of Nakaoka et al. (2006) for 1997–2001. Our estimates are also in phase with the biogeochemical ocean modeling result of Manizza et al. (2013) for the Arctic during 1996–2007, although their CO_2 influxes were weaker than most other estimates, including ours, as mentioned in Section 4.1.

5. Concluding remarks

By applying, for the first time, a SOM technique to $p\text{CO}_{2w}$ estimation in the Arctic, we produced monthly maps of air–sea CO_2 fluxes from 1997 to 2013 for the Arctic north of 60°N , including the Arctic Ocean and its adjacent seas. These maps cover a larger area over a longer period than previous regression-based estimates of Arctic air–sea CO_2 fluxes. Using the mapped result, we were able to comprehensively describe the spatiotemporal distribution of the CO_2 flux variability on seasonal and interannual time scales. The monthly CO_2 flux data presented in this paper are available at the JAMSTEC web page (<http://www.jamstec.go.jp/res/ress/yasunaka/co2flux/>).

Although in the present study we estimated CO_2 fluxes for the entire ocean area of the Arctic, observations in the Kara, Laptev, and East Siberian Seas and the Eurasian Basin were too scarce to determine seasonal and interannual variabilities there. To improve our understanding of the variability in air–sea CO_2 fluxes in the Arctic, it is of critical importance to fill the large spatial and temporal data gaps by obtaining additional ocean CO_2 measurements. The availability of monthly fields for mixed layer depth and chlorophyll would also improve the mapping of the $p\text{CO}_{2w}$ field and thereby further clarify the air–sea CO_2 flux variability.

Acknowledgments

This work was financially supported by the Green Network of Excellence (GRENE) Arctic Climate Change Research Project of the Ministry of Education, Culture, Sports, Science and Technology of Japan. We are grateful to Maciej Telszewski of Institute of Oceanology of Polish Academy of Sciences and Shin-ichiro Nakaoka of National Institute for Environmental Studies for providing their mapping codes for our reference. A. M. and D. S. also acknowledge support from JSPS KAKENHI Grant Number 23241002. A. M. O. is

supported by the Centre for Climate Dynamics at the Bjerknes Centre. A. O. appreciates support from the Norwegian Research Council (project SNACS, 229752). T. T. and the $p\text{CO}_2$ measurements aboard the USCGC *Healy*, R/V *N. Palmer*, and R/V *M. Langseth* were supported by a grant (NA10OAR4320143) from the Ship of Opportunity Program (SOOP) of NOAA. M.H. was partly supported by the German Integrated Carbon Observation System (ICOS-D; grant 01LK1224I). We used the CO2SYS program obtained from the Carbon Dioxide Information Analysis Center (<http://cdiac.ornl.gov/oceans/co2rprt.html>), and SOM Toolbox Version 2 developed by the Laboratory of Information and Computer Science at Helsinki University of Technology (<http://www.cis.hut.fi/projects/somtoolbox>).

Appendix A. Supplementary data

Supplementary data related to this article can be found at <http://dx.doi.org/10.1016/j.polar.2016.03.006>.

References

- Arrigo, K.R., Pabi, S., van Dijken, G.L., Maslowski, W., 2010. Air–sea flux of CO_2 in the Arctic Ocean, 1998–2003. *J. Geophys. Res.* 115, G04024. <http://dx.doi.org/10.1029/2009JG001224>.
- Anderson, L.G., Drange, H., Chierici, M., Fransson, A., Johannessen, T., Skjelvan, I., Rey, F., 2000. Annual carbon fluxes in the upper Greenland Sea based on measurements and a box-model approach. *Tellus* 52B, 1013–1024.
- Bakker, D.C.E., Pfeil, B., Smith, K., Hankin, S., Olsen, A., Alin, S.R., Cosca, C., Harasawa, S., Kozyr, A., Nojiri, Y., O'Brien, K.M., Schuster, U., Telszewski, M., Tilbrook, B., Wada, C., Akl, J., Barbero, L., Bates, N., Boutin, J., Cai, W.-J., Castle, R.D., Chavez, F.P., Chen, L., Chierici, M., Currie, K., de Baar, H.J.W., Evans, W., Feely, R.A., Fransson, A., Gao, Z., Hales, B., Hardman-Mountford, N., Hoppema, M., Huang, W.-J., Hunt, C.W., Huss, B., Ichikawa, T., Johannessen, T., Jones, E.M., Jones, S., Jutterström, Sara, Kitidis, V., Körtzinger, A., Lauvset, S.K., Lefèvre, N., Manke, A.B., Mathis, J.T., Merlivat, L., Metzl, N., Murata, A., Newberger, T., Ono, T., Park, G.-H., Paterson, K., Pierrot, D., Ríos, A.F., Sabine, C.L., Saito, S., Salisbury, J., Sarma, V.V.S.S., Schlitzer, R., Sieger, R., Skjelvan, I., Steinhoff, T., Sullivan, K., Sun, H., Sutton, A.J., Suzuki, T., Sweeney, C., Takahashi, T., Tjiputra, J., Tsurushima, N., van Heuven, S.M.A.C., Vandemark, D., Vlahos, P., Wallace, D.W.R., Wanninkhof, R., Watson, A.J., 2014. An update to the Surface Ocean CO₂ Atlas (SOCAT version 2). *Earth Syst. Sci. Data* 6, 1–22. <http://dx.doi.org/10.5194/essd-6-69-2014>.
- Bakker, D.C.E., Pfeil, B., Smith, K., Harasawa, S., Landa, C., Nakaoka, S., Nojiri, Y., Metzl, N., O'Brien, K.M., Olsen, A., Schuster, U., Tilbrook, B., Wanninkhof, R., Alin, S.R., Barbero, L., Bates, N.R., Bianchi, A.A., Bonou, F., Boutin, J., Bozec, Y., Burger, E., Cai, W.-J., Castle, R.D., Chen, L., Chierici, M., Cosca, C., Currie, K., Evans, W., Featherstone, C., Feely, R.A., Fransson, A., Greenwood, N., Gregor, L., Hankin, S., Hardman-Mountford, N.J., Harlay, J., Hauck, J., Hoppema, M., Humphreys, M., Hunt, C.W., Ibáñez, J.S.P., Johannessen, T., Jones, S.D., Keeling, R., Kitidis, V., Körtzinger, A., Kozyr, A., Krasakopoulou, E., Kuwata, A., Landschützer, P., Lauvset, S.K., Lefèvre, N., Lo Monaco, C., Manke, A.B., Mathis, J.T., Merlivat, L., Monteiro, P., Munro, D., Murata, A., Newberger, T., Omar, A.M., Ono, T., Paterson, K., Pierrot, D., Robbins, L.L., Sabine, I., Saito, S., Salisbury, J., Schneider, B., Schlitzer, R., Sieger, R., Skjelvan, I., Steinhoff, T., Sullivan, K.F., Sutherland, S.C., Sutton, A.J., Sweeney, C., Tadokoro, K., Takahashi, T., Telszewski, M., Van Heuven, S.M.A.C., Vandemark, D., Wada, C., Ward, B., Watson, A.J., 2016. A 58-year Record of High Quality Data in Version 3 of the Surface Ocean CO₂ Atlas (SOCAT) (In preparation for Earth System Science Data).
- Bates, N.R., Mathis, J.T., 2009. The Arctic Ocean marine carbon cycle: evaluation of air–sea CO_2 exchanges, ocean acidification impacts and potential feedbacks. *Biogeosciences* 6, 2433–2459. <http://dx.doi.org/10.5194/bg-6-2433-2009>.
- Bates, N.R., Best, M.H.P., Hansell, D.A., 2005. Spatio-temporal distribution of dissolved inorganic carbon and net community production in the Chukchi and Beaufort Seas. *Deep-Sea Res. Part II Top. Stud. Oceanogr.* 52 (24–26), 3303–3323. <http://dx.doi.org/10.1016/j.dsr2.2005.10.005>.
- Bates, N.R., Moran, S.B., Hansell, D.A., Mathis, J.T., 2006. An increasing CO_2 sink in the Arctic Ocean due to sea-ice loss. *Geophys. Res. Lett.* 33, L23609. <http://dx.doi.org/10.1029/2006GL027028>.
- Bates, N.R., Garley, R., Frey, K.E., Shake, K.L., Mathis, J.T., 2014. Sea-ice melt CO_2 -carbonate chemistry in the western Arctic Ocean: meltwater contributions to air–sea CO_2 gas exchange, mixed layer properties and rates of net community production under sea ice. *Biogeosciences* 11, 6769–6789. <http://dx.doi.org/10.5194/bg-11-6769-2014>.
- Cai, W.J., Chen, L.Q., Chen, B.S., Gao, Z.Y., Lee, S.H., Chen, J.F., Pierrot, D., Sullivan, K., Wang, Y.C., Hu, X.P., Huang, W.J., Zhang, Y.H., Xu, S.Q., Murata, A., Grebeier, J.M., Jones, E.P., Zhang, H.S., 2010. Decrease in the CO_2 uptake capacity in an ice-free Arctic Ocean Basin. *Science* 329, 556–559.

- Cavaliere, D.J., Gloersen, P., Campbell, W.J., 1984. Determination of sea ice parameters with the NIMBUS-7 SMMR. *J. Geophys. Res.* 89, 5355–5369.
- Ciais, P., Sabine, C., Bala, G., Bopp, L., Brovkin, V., Canadell, J., Chhabra, A., DeFries, R., Galloway, J., Heimann, M., Jones, C., Le Quéré, C., Myneni, R.B., Piao, S., Thornton, P., 2013. Carbon and other Biogeochemical cycles. In: Stocker, T.F., Qin, D., Plattner, G.-K., Tignor, M., Allen, S.K., Boschung, J., Nauels, A., Xia, Y., Bex, V., Midgley, P.M. (Eds.), *Climate Change 2013: the Physical Science Basis. Contribution of Working Group I to the Fifth Assessment Report of the Intergovernmental Panel on Climate Change*. Cambridge University Press, Cambridge, United Kingdom and New York, NY, USA.
- Conway, T.J., Tans, P.P., Waterman, L.S., Thoning, K.W., Kitzis, D.R., Masarie, K.A., Zhang, N., 1994. Evidence for interannual variability of the carbon cycle from the NOAA/CMDL global air sampling network. *J. Geophys. Res.* 99, 22831–22855.
- Cota, G.F., Pomeroy, L.R., Harrison, W.G., Jones, E.P., Peters, F., Sheldon, W.M., Weingartner, T.R., 1996. Nutrients, primary production and microbial heterotrophy in the Southeastern Chukchi Sea: Arctic summer nutrient depletion and heterotrophy. *Mar. Ecol. Prog. Ser.* 135, 247–258.
- Dickson, A.G., 1990. Standard potential of the reaction: $\text{AgCl(s)} + 1/2 \text{H}_2(\text{g}) = \text{Ag(s)} + \text{HCl(aq)}$, and the standard acidity constant of the ion HSO_4^- in synthetic seawater from 273.15 to 318.15 K. *J. Chem. Thermodyn.* 22, 113–127.
- Else, B.G.T., Galley, R.J., Lansard, B., Barber, D.G., Brown, K., Miller, L.A., Mucci, A., Papakyriakou, T.N., Tremblay, J.-É., Rysgaard, S., 2013. Further observations of a decreasing atmospheric CO_2 uptake capacity in the Canada Basin (Arctic Ocean) due to sea ice loss. *Geophys. Res. Lett.* 40, 1132–1137. <http://dx.doi.org/10.1002/grl.50268>.
- Evans, W., Mathis, J.T., Cross, J.N., Bates, N.R., Frey, K.E., Else, B.G.T., Papakyriakou, T.N., DeGrandpre, M.D., Islam, F., Cai, W.-J., Chen, B., Yamamoto-Kawai, M., Carmack, E., Williams, W.J., Takahashi, T., 2015. Sea-air CO_2 exchange in the western Arctic coastal ocean. *Glob. Biogeochem. Cycles* 29, 1190–1209. <http://dx.doi.org/10.1002/2015GB005153>.
- Fransson, A., Chierici, M., Anderson, L.C., Bussmann, I., Kattner, G., Jones, E.P., Swift, J.H., 2001. The importance of shelf processes for the modification of chemical constituents in the waters of the Eurasian Arctic Ocean: implication for carbon fluxes. *Cont. Shelf Res.* 21, 225–242.
- Gao, Z., Chen, L., Sun, H., Chen, B., Cai, W.-J., 2012. Distributions and air–sea fluxes of carbon dioxide in the Western Arctic Ocean. *Deep-Sea Res. II* 81–84, 46–52. <http://dx.doi.org/10.1016/j.dsr2.2012.08.021>.
- Giesbrecht, K.E., Miller, L.A., Zimmermann, S., Carmack, E., Johnson, W.K., Macdonald, R.W., McLaughlin, F., Mucci, A., Williams, W.J., Wong, C.S., Yamamoto-Kawai, M., 2013. Measurements of the Dissolved Inorganic Carbon System and Associated Biogeochemical Parameters in the Canadian Arctic, 1974–2009. Carbon Dioxide Information Analysis Center, Oak Ridge National Laboratory, US Department of Energy, Oak Ridge, Tennessee. http://dx.doi.org/10.3334/CDIAC/OTG.IOSaRCT_CARBN. http://cdiac.ornl.gov/ftp/oceans/IOSaRct_Database/
- Gloersen, P., Campbell, W.J., Cavaliere, D.J., Comiso, J.C., Parkinson, C.L., Zwally, H.J., 1993. Arctic and Antarctic sea ice, 1978–1987: satellite passive-microwave observations and analysis. *NASA Spec. Publ.* 511, 290.
- Gruber, N., Gloor, M., Mikaloff Fletcher, S.E., Dutkiewicz, S., Follows, M., Doney, S.C., Gerber, M., Jacobson, A.R., Lindsay, K., Menemenlis, D., Mouchet, A., Mueller, S.A., Sarmiento, J.L., Takahashi, T., 2009. Oceanic sources and sinks for atmospheric CO_2 . *Glob. Biogeochem. Cycles* 23, GB1005. <http://dx.doi.org/10.1029/2008GB003349>.
- Jutterström, S., Anderson, L.G., Bates, N.R., Bellerby, R., Johannessen, T., Jones, E.P., Key, R.M., Lin, X., Olsen, A., Omar, A.M., 2010. Arctic Ocean data in CARINA. *Earth Syst. Sci. Data* 2, 71–78.
- Kaltin, S., Anderson, L.G., 2005. Uptake of atmospheric carbon dioxide in Arctic shelf seas: evaluation of the relative importance of processes that influence pCO_2 in water transported over the Bering–Chukchi Sea shelf. *Mar. Chem.* 94, 67–79. <http://dx.doi.org/10.1016/j.marchem.2004.07.010>.
- Kaltin, S., Anderson, L.G., Olsson, K., Fransson, A., Chierici, M., 2002. Uptake of atmospheric carbon dioxide in the Barents Sea. *J. Mar. Syst.* 38, 31–45. [http://dx.doi.org/10.1016/S0924-7963\(02\)00168-9](http://dx.doi.org/10.1016/S0924-7963(02)00168-9).
- Kanamitsu, M., Ebisuzaki, W., Woollen, J., Yang, S.-K., Hnilo, J.J., Fiorino, M., Potter, G.L., 2002. NCEP–DOE AMIP-II reanalysis (R-2). *Bull. Am. Meteor. Soc.* 83, 1631–1643.
- Key, R.M., Kozyr, A., Sabine, C.L., Lee, K., Wanninkhof, R., Bullister, J., Feely, R.A., Millero, F., Mordy, C., Peng, T.-H., 2004. A Global Ocean carbon climatology: results from global data analysis project (GLODAP). *Glob. Biogeochem. Cycles* 18, GB4031. <http://dx.doi.org/10.1029/2004GB002247>.
- Key, R.M., Tanhua, T., Olsen, A., Hoppema, M., Jutterström, S., Schirnick, C., van Heuven, S., Kozyr, A., Lin, X., Velo, A., Wallace, D.W.R., Mintrop, L., 2010. The CARINA data synthesis project: introduction and overview. *Earth Syst. Sci. Data* 2, 105–121. <http://dx.doi.org/10.5194/essd-2-105-2010>.
- Land, P.E., Shutler, J.D., Cowling, R.D., Woolf, D.K., Walker, P., Findlay, H.S., Upstill-Goddard, R.C., Donlon, C.J., 2013. Climate change impacts on sea–air fluxes of CO_2 in three Arctic seas: a sensitivity study using Earth observation. *Biogeosciences* 10, 8109–8128. <http://dx.doi.org/10.5194/bg-10-8109-2013>.
- Landschützer, P., Gruber, N., Bakker, D.C.E., Schuster, U., 2014. Recent variability of the global ocean carbon sink. *Glob. Biogeochem. Cycles* 28, 927–949. <http://dx.doi.org/10.1002/2014GB004853>.
- Lauvset, S.K., Chierici, M., Counillon, F., Omar, A.M., Nondal, G., Johannessen, T., Olsen, A., 2013. Annual and seasonal fCO_2 and air–sea CO_2 fluxes in the Barents Sea. *J. Mar. Syst.* 113–114, 62–74. <http://dx.doi.org/10.1016/j.jmarsys.2012.12.011>.
- Lefèvre, N., Watson, A.J., Watson, A.R., 2005. A comparison of multiple regression and neural network techniques for mapping in situ pCO_2 data. *Tellus B* 57, 375–384. <http://dx.doi.org/10.1111/j.1600-0889.2005.00164.x>.
- Lewis, E., Wallace, D.W.R., 1998. Program Developed for CO_2 System Calculations. ORNL/CDIAC-105. Carbon Dioxide Information Analysis Center, Oak Ridge National Laboratory, U.S. Department of Energy, Oak Ridge, Tennessee.
- Loose, B., McGillis, W.R., Schlosser, P., Perovich, D., Takahashi, T., 2009. Effects of freezing, growth, and ice cover on gas transport processes in laboratory seawater experiments. *Geophys. Res. Lett.* 36, L05603. <http://dx.doi.org/10.1029/2008GL036318>.
- Lueker, T.J., Dickson, A.G., Keeling, C.D., 2000. Ocean pCO_2 calculated from dissolved inorganic carbon, alkalinity, and equations for K_1 and K_2 : validation based on laboratory measurements of CO_2 in gas and seawater at equilibrium. *Mar. Chem.* 70, 105–119.
- Manizza, M., Follows, M.J., Dutkiewicz, S., Menemenlis, D., Hill, C.N., Key, R.M., 2013. Changes in the Arctic Ocean CO_2 sink (1996–2007): a regional model analysis. *Glob. Biogeochem. Cycles* 27, 1108–1118. <http://dx.doi.org/10.1002/2012GB004491>.
- Meier, W., Fetterer, F., Savoie, M., Mallory, S., Duerr, R., Stroeve, J., 2013. NOAA/NSIDC Climate Data Record of Passive Microwave Sea Ice Concentration. Version 2 [Measurements of the Dissolved Indicate Subset Used]. National Snow and Ice Data Center, Boulder, Colorado USA. <http://dx.doi.org/10.7265/N55M63M1>.
- Murata, A., Takizawa, T., 2003. Summertime CO_2 sink in shelf and slope waters of the western Arctic Ocean. *Cont. Shelf Res.* 23, 753–776.
- Murray, F.W., 1967. On the computation of saturation vapor pressure. *J. Appl. Meteorol.* 6, 203–204.
- Nakaoka, S.-I., Aoki, S., Nakazawa, T., Hashida, G., Morimoto, S., Yamanouchi, T., Yoshikawa-Inoue, H., 2006. Temporal and spatial variations of oceanic pCO_2 and air–sea CO_2 flux in the Greenland Sea and the Barents Sea. *Tellus B* 58, 148–161. <http://dx.doi.org/10.1111/j.1600-0889.2006.00178.x>.
- Nakaoka, S., Telszewski, M., Nojiri, Y., Yasunaka, S., Miyazaki, C., Mukai, H., Usui, N., 2013. Estimating temporal and spatial variation of sea surface pCO_2 in the North Pacific using a self organizing map neural network technique. *Biogeosciences* 10, 6093–6106. <http://dx.doi.org/10.5194/bg-10-6093-2013>.
- Olsen, A., Bellerby, R.G.J., Johannessen, T., Omar, A.M., Skjelvan, I., 2003. Interannual variability in the wintertime air–sea flux of carbon dioxide in the northern North Atlantic, 1981–2001. *Deep-Sea Res. I* 50 (10–11), 1323–1338. [http://dx.doi.org/10.1016/S0967-0637\(03\)00144-4](http://dx.doi.org/10.1016/S0967-0637(03)00144-4).
- Omar, A.M., Johannessen, T., Olsen, A., Kaltin, S., 2007. Seasonal and interannual variability of the air–sea CO_2 flux in the Atlantic sector of the Barents Sea. *Mar. Chem.* 104, 203–213. <http://dx.doi.org/10.1016/j.marchem.2006.11.002>.
- Peng, G., Meier, W., Scott, D., Savoie, M., 2013. A long-term and reproducible passive microwave sea ice concentration data record for climate studies and monitoring. *Earth Syst. Sci. Data* 5, 311–318. <http://dx.doi.org/10.5194/essd-5-311-2013>.
- Pfeil, B., Olsen, A., Bakker, D.C.E., Hankin, S., Koyuk, H., Kozyr, A., Malczyk, J., Manke, A., Metzl, N., Sabine, C.L., Akl, J., Alin, S.R., Bates, N., Bellerby, R.G.J., Borges, A., Boutin, J., Brown, P.J., Cai, W.-J., Chavez, F.P., Chen, A., Cosca, C., Fassbender, A.J., Feely, R.A., González-Dávila, M., Goyet, C., Hales, B., Hardman-Mountford, N., Heinze, C., Hood, M., Hoppema, M., Hunt, C.W., Hydes, D., Ishii, M., Johannessen, T., Jones, S.D., Key, R.M., Körtzinger, A., Landschützer, P., Lauvset, S.K., Lefèvre, N., Lenton, A., Lourantou, A., Merlivat, L., Midorikawa, T., Mintrop, L., Miyazaki, C., Murata, A., Nakadate, A., Nakano, Y., Nakaoka, S., Nojiri, Y., Omar, A.M., Padin, X.A., Park, G.-H., Paterson, K., Perez, F.F., Pierrot, D., Poisson, A., Ríos, A.F., Santana-Casiano, J.M., Salisbury, J., Sarma, V.V.S.S., Schlitzer, R., Schneider, B., Schuster, U., Sieger, R., Skjelvan, I., Steinhoff, T., Suzuki, T., Takahashi, T., Tedesco, K., Telszewski, M., Thomas, H., Tilbrook, B., Tjiputra, J., Vandemark, D., Veness, T., Wanninkhof, R., Watson, A.J., Weiss, R., Wong, C.S., Yoshikawa-Inoue, H., 2013. A uniform, quality controlled Surface Ocean CO_2 Atlas (SOCAT). *Earth Syst. Sci. Data* 5, 125–143. <http://dx.doi.org/10.5194/essd-5-125-2013>.
- Reynolds, R.W., Rayner, N.A., Smith, T.M., Stokes, D.C., Wang, W., 2002. An improved in situ and satellite SST analysis for climate. *J. Clim.* 15, 1609–1625.
- Schuster, U., McKinley, G.A., Bates, N., Chevallier, F., Doney, S.C., Fay, A.R., González-Dávila, M., Gruber, N., Jones, S., Krijnen, J., Landschützer, P., Lefèvre, N., Manizza, M., Mathis, J., Metzl, N., Olsen, A., Ríos, A.F., Rödenbeck, C., Santana-Casiano, J.M., Takahashi, T., Wanninkhof, R., Watson, A.J., 2013. An assessment of the Atlantic and Arctic sea–air CO_2 fluxes, 1990–2009. *Biogeosciences* 10, 607–627. <http://dx.doi.org/10.5194/bg-10-607-2013>.
- Semiletov, I., Makshtas, A., Akasofu, S.-I., Andreas, E.L., 2004. Atmospheric CO_2 balance: the role of Arctic sea ice. *Geophys. Res. Lett.* 31, L05121. <http://dx.doi.org/10.1029/2003GL017996>.
- Signorini, S.R., McClain, C.R., 2009. Effect of uncertainties in climatologic wind, ocean pCO_2 , and gas transfer algorithms on the estimate of global sea–air CO_2 flux. *Glob. Biogeochem. Cycles* 23, GB2025. <http://dx.doi.org/10.1029/2008GB003246>.
- Steele, M., Morley, R., Ermold, W., 2001. PHC: a global ocean hydrography with a high quality Arctic Ocean. *J. Clim.* 14, 2079–2087.
- Sweeney, C., Gloor, E., Jacobson, A.R., Key, R.M., McKinley, G., Sarmiento, J.L., Wanninkhof, R., 2007. Constraining global air–sea gas exchange for CO_2 with recent bomb ^{14}C measurements. *Glob. Biogeochem. Cycles* 21, GB2015. <http://dx.doi.org/10.1029/2006GB002784>.
- Takahashi, T., Sutherland, S.C., Wanninkhof, R., Sweeney, C., Feely, R.A., Chipman, D.W., Hales, B., Friederich, G., Chavez, F., Sabine, C., Watson, A., Bakker, D.C.E., Schuster, U., Metzl, N., Yoshikawa-Inoue, H., Ishii, M.,

- Midorikawa, T., Nojiri, Y., Körtzinger, A., Steinhoff, T., Hoppema, M., Olafsson, J., Arnarson, T.S., Tilbrook, B., Johannessen, T., Olsen, A., Bellerby, R., Wong, C.S., Delille, B., Bates, N.R., de Baar, H.J.W., 2009. Climatological mean and decadal changes in surface ocean pCO₂, and net sea-air CO₂ flux over the global oceans. *Deep-Sea Res. II* 56, 554–577.
- Takahashi, T., Sutherland, S.C., Kozyr, A., 2015. Global Ocean Surface Water Partial Pressure of CO₂ Database: Measurements Performed during 1957–2014 (Version 2014). ORNL/CDIAC-160, NDP-088(V2014). Carbon Dioxide Information Analysis Center, Oak Ridge National Laboratory, U.S. Department of Energy, Oak Ridge, Tennessee. [http://dx.doi.org/10.3334/CDIAC/OTG.NDP088\(V2014\)](http://dx.doi.org/10.3334/CDIAC/OTG.NDP088(V2014)).
- Tanhua, T., Olsen, A., Hoppema, M., Jutterström, S., Schirnack, C., van Heuven, S., Velo, A., Lin, X., Kozyr, A., Alvarez, M., Bakker, D.C.E., Brown, P., Falck, E., Jeansson, E., Lo Monaco, C., Olafsson, J., Perez, F.F., Pierrot, D., Rios, A.F., Sabine, C.L., Schuster, U., Steinfeldt, R., Stendardo, I., Anderson, L.G., Bates, N.R., Bellerby, R.G.J., Blindheim, J., Bullister, J.L., Gruber, N., Ishii, M., Johannessen, T., Jones, E.P., Köhler, J., Körtzinger, A., Metzl, N., Murata, A., Musielewicz, S., Omar, A.M., Olsson, K.A., de la Paz, M., Pfeil, B., Rey, F., Rhein, M., Skjelvan, I., Tilbrook, B., Wanninkhof, R., Mintrop, L., Wallace, D.W.R., Key, R.M., 2009. CARINA Data Synthesis Project. ORNL/CDIAC-157, NDP-091. Carbon Dioxide Information Analysis Center, Oak Ridge National Laboratory, U.S. Department of Energy, Oak Ridge, Tennessee. <http://dx.doi.org/10.3334/CDIAC/otg.ndp091>.
- Telszewski, M., Chazottes, A., Schuster, U., Watson, A.J., Moulin, C., Bakker, D.C.E., González-Dávila, M., Johannessen, T., Körtzinger, A., Lüger, H., Olsen, A., Omar, A., Padin, X.A., Ríos, A.F., Steinhoff, T., Santana-Casiano, M., Wallace, D.W.R., Wanninkhof, R., 2009. Estimating the monthly pCO₂ distribution in the North Atlantic using a self-organizing neural network. *Biogeosciences* 6, 1405–1421. <http://dx.doi.org/10.5194/bg-6-1405-2009>.
- van Heuven, S., Pierrot, D., Lewis, E., Wallace, D.W.R., 2009. MATLAB Program Developed for CO₂ System Calculations, ORNL/CDIAC-105b. Carbon Dioxide Information Analysis Center, Oak Ridge National Laboratory, US Department of Energy, Oak Ridge, Tennessee.
- Wanninkhof, R., 1992. Relationship between wind speed and gas exchange over the ocean. *J. Geophys. Res.* 97 (C5), 7373–7382. <http://dx.doi.org/10.1029/92JC00188>.
- Wanninkhof, R., 2014. Relationship between wind speed and gas exchange over the ocean revisited. *Limnol. Oceanogr. Methods* 12, 351–362.
- Wanninkhof, R., Park, G.-H., Takahashi, T., Sweeney, C., Feely, R., Nojiri, Y., Gruber, N., Doney, S.C., McKinley, G.A., Lenton, A., Le Quéré, C., Heinze, C., Schwinger, J., Graven, H., Khattiwala, S., 2013. Global ocean carbon uptake: magnitude, variability and trends. *Biogeosciences* 10, 1983–2000. <http://dx.doi.org/10.5194/bg-10-1983-2013>.
- Weiss, R.F. (1974), Carbon dioxide in water and seawater: the solubility of a non-ideal gas, *Marine Chemistry*, 2, 203–215.
- Weiss, R.F., 1974. Carbon dioxide in water and seawater: the solubility of a non-ideal gas. *Mar. Chem.* 2, 203–215.
- Yasunaka, S., Nojiri, Y., Nakaoka, S., Ono, T., Whitney, F.A., Telszewski, M., 2014. Mapping of sea surface nutrients in the North Pacific: Basin-wide distribution and seasonal to interannual variability. *J. Geophys. Res. Oceans* 119, 7756–7771. <http://dx.doi.org/10.1002/2014JC010318>.